CMS Physics Analysis Summary

Contact: cms-pag-conveners-higgs@cern.ch 2019/03/17

Search for a heavy pseudoscalar Higgs boson decaying into a 125 GeV Higgs boson and a Z boson in final states of two light leptons and two tau leptons at $\sqrt{s} = 13$ TeV

The CMS Collaboration

Abstract

A search is performed for a pseudoscalar Higgs boson, A, decaying into a standard model-like Higgs boson h and a Z boson. The standard model-like Higgs boson is specifically targeted in its decay into a pair of tau leptons, while the Z boson decays leptonically. A data sample of proton-proton collisions collected at $\sqrt{s} = 13$ TeV by the CMS experiment at the LHC is used, and corresponds to an integrated luminosity of 35.9 fb^{-1}. In the absence of observing the signal, model-independent and model-dependent limits are set. The model-dependent limits are set in two minimal supersymmetric standard model benchmark scenarios in the m_{A}-tan β plane.

1 Introduction

In the standard model (SM) [1, 2], the Brout–Englert–Higgs mechanism [3–8] is responsible for electroweak symmetry breaking, and it predicts the existence of the Higgs boson. A Higgs boson was discovered by the ATLAS and CMS Collaborations in the ZZ, $\gamma\gamma$, and WW channels [9–11]. Its mass is determined to be $m_{\mathrm{h}} = 125.26 \pm 0.20\,(\mathrm{stat}) \pm 0.08\,(\mathrm{syst})\,\mathrm{GeV}$ based on data collected by the CMS experiment at a center-of-mass energy of 13 TeV [12]. This is consistent with other measurements by the ATLAS and CMS experiments, including their combined results [13, 14]. Additionally, the properties of the observed boson, such as couplings to fermions, have been studied extensively, and are found to be compatible with the SM expectation [15, 16].

The observation of the SM-like Higgs boson has not only given closure for the hunt for particles described by the SM, but also constrains the beyond standard model theories proposed to explain some of the open questions in particle physics. A class of simple extensions of the SM, two-Higgs-doublet models (2HDMs), predict five Higgs bosons [17, 18]. One of these five particles, the light CP-even Higgs boson h, could correspond to the observed particle. The mass of the observed state can be used to exclude regions of the parameter space of 2HDMs, and the rest of it can be constrained by performing searches for the additional four Higgs bosons, namely the heavy CP-even Higgs boson H, the CP-odd Higgs boson A, and two charged Higgs bosons $\mathrm{H}^{\pm}$. The parameter space is often described by two parameters: the ratio of the vacuum expectation values of the two doublets ($\tan\beta = v_2/v_1$) and the mass of the CP-odd pseudoscalar A (m_{A}). Another parameter, the mixing angle α, is defined for the CP-even scalars h and H. The parameters α and β determine the interactions between the Higgs field and the vector bosons and the fermions, offering a categorisation of possible types of 2HDMs based on the couplings of the two doublets to fermions and vector bosons. The most studied type of 2HDMs is type II as the Minimal supersymmetric standard model (MSSM) is a special case of this. In the MSSM the couplings of h (H) to vector bosons are normalized to the SM couplings by $\sin(\beta-\alpha)$ ($\cos(\alpha-\beta)$).

In this note, we study two MSSM benchmark scenarios: Low $\tan\beta$ and hMSSM [19–21]. In the MSSM when the mass of the h boson is close to 125 GeV, the scale of the soft supersymmetry breaking masses must be larger than 1 TeV. This is a reasonable assumption based on the non-observations of supersymmetric particles at the LHC thus far. In the hMSSM scenario, by requiring $m_{\mathrm{h}} = 125\,\mathrm{GeV}$, the dominant radiative corrections to the Higgs boson masses become fixed. As a result, the MSSM Higgs sector can be described to a good approximation by $\tan\beta$ and m_{A} without fixing other parameters of the theory, such as α, m_{H}, and $m_{\mathrm{H}^{\pm}}$. In contrast to the hMSSM scenario, the Low $\tan\beta$ scenario is based on choosing the supersymmetric parameters so that the observed value of m_{h} is obtained in most of the m_{A}–$\tan\beta$ plane. The radiative corrections to the Higgs boson masses are included in this case. To explore the parameter space of these benchmark scenarios, we choose an experimentally accessible final state with at least one SM-like Higgs boson. In the phase space region with low $\tan\beta$ values, the pseudoscalar A boson has a substantial branching fraction into a SM-like Higgs boson h and a Z boson.

This note reports on a search for the pseudoscalar A boson decaying into a SM-like Higgs boson h and a Z boson in proton-proton (pp) collisions at $\sqrt{s} = 13\,\mathrm{TeV}$. The search uses a data set collected in 2016 by the CMS experiment corresponding to an integrated luminosity of $35.9\,\mathrm{fb}^{-1}$. The studied signal mass range begins at 220 GeV because the A boson must be massive enough to decay into the considered Zh state. The mass range extends up to 400 GeV, slightly above where the mass of the A boson exceeds twice the top quark mass. This is where the decay $\mathrm{A} \to \mathrm{tt}$ starts to dominate.

In this search, the SM-like Higgs boson is sought in its decay into a pair of tau leptons. Previous searches covering this process have been performed by the ATLAS and CMS Collaborations using data sets collected in pp collisions at $\sqrt{s} = 8\,\text{TeV}$ [22, 23]. These analyses set both model-independent and model-dependent limits in the context of type-II 2HDMs. The CMS Collaboration also set model-dependent limits in the Low $\tan\beta$ scenario discussed above. The ATLAS and CMS Collaborations have also searched for the pseudoscalar A decaying into the same intermediate Zh state but with the Higgs boson h decaying into a pair of bottom quarks in pp collisions at $\sqrt{s} = 13\,\text{TeV}$ [24, 25].

Four possible $\tau\tau$ decay channels of the SM-like Higgs boson are considered: $\text{e}\tau_\text{h}$, $\mu\tau_\text{h}$, $\text{e}\mu$, and $\tau_\text{h}\tau_\text{h}$, where τ_h denotes a tau lepton decaying hadronically. Throughout the note neutrinos are omitted from the notation of the final states. These four decay channels are combined with the Z boson decays into two leptons via $\text{Z} \to \ell^+\ell^-$ ($\ell = \text{e}, \mu$), resulting in eight distinct final states of the A boson decay. To account for the missing energy that results from the neutrinos in the final states, we use the SVFIT algorithm [26] to reconstruct the 4-vector of the SM-like Higgs boson while constraining its mass to 125 GeV. Compared to the previous result presented by the CMS Collaboration [23], this approach, which constrains the SM-like Higgs boson mass, significantly increases the sensitivity of the search.

2 The CMS detector

The central feature of the CMS apparatus is a superconducting solenoid of 6 m internal diameter, providing a magnetic field of 3.8 T. Within the solenoid volume are a silicon pixel and strip tracker, a lead tungstate crystal electromagnetic calorimeter (ECAL), and a brass and scintillator hadron calorimeter, each composed of a barrel and two endcap sections. Forward calorimeters extend the pseudorapidity (η) coverage provided by the barrel and endcap detectors. Muons are detected in gas-ionization chambers embedded in the steel flux-return yoke outside the solenoid. Events of interest are selected using a two-tiered trigger system [27]. A more detailed description of the CMS detector, together with a definition of the coordinate system used and the relevant kinematic variables, can be found in Ref. [28].

3 Simulated samples

Simulated signal events with a pseudoscalar Higgs boson A produced in gluon fusion (ggA), decaying into a SM-like Higgs boson and a Z boson and finally into two light leptons (electrons or muons) and two tau leptons are generated at leading order (LO) using MADGRAPH5_aMC@NLO v2.3.3 [29]. The considered A boson mass points are within 220–400 GeV, as in this mass range the decay into a Z boson and a h boson is the dominating decay mode. The samples are based on the $m_\text{h}^{\text{mod}+}$ model [21], assuming a low value of $\tan\beta$ ($\sim$ 2). The generated width of the A is narrow for all masses compared to the experimental resolution. Additional signal events are simulated for a 300 GeV A boson produced in association with b quarks (bbA) and are used only to study the selection efficiency, necessary for setting model-dependent limits as explained later on in Section 8.

The background processes consist of all SM processes with non-negligible yield in the studied final states, including the Higgs boson production through processes predicted in the SM (e.g. Zh, Wh, $\text{t}\bar{\text{t}}\text{h}$). The background processes with a Higgs boson decaying into two tau leptons, produced in association with a W or Z boson (Wh or Zh) are generated at next-to-LO (NLO) in perturbative quantum chromodynamics (QCD) with the POWHEG 2.0 [30–34] generator extended with the MiNLO procedure [35]. The contribution from Higgs boson events pro-

duced via gluon fusion or vector boson fusion and decaying into two tau leptons is negligible. The transverse momentum (p_T) distribution of the Higgs boson in the POWHEG simulations is tuned to match closely the next-to-NLO plus next-to-next-to-leading-logarithmic prediction in the HRES 2.3 generator [36, 37]. The production cross sections and branching fractions for the SM Higgs boson production and their corresponding uncertainties are taken from Refs. [38–40].

The background samples for $t\bar{t}h$, $t\bar{t}$, WZ, and $qq \to ZZ$, as well as $Wh \to WWW$, $Wh \to WZZ$, $Zh \to ZWW$, $Zh \to ZZZ$, and $ggh \to ZZ$ processes, are generated at NLO with POWHEG. The $gg \to ZZ$ process is generated at LO with MCFM [41]. Samples for the $qq \to ZZ$ and $gg \to ZZ$ processes include all SM events with two Z bosons in final states except the ones from $ggh \to ZZ$ process. The MADGRAPH5_aMC@NLO v2.3.3 generator is used for triboson, $t\bar{t}W$, and $t\bar{t}Z$ production, with the jet matching and merging scheme applied either at NLO with the FxFx algorithm [42] or at LO with the MLM algorithm [43]. The generators are interfaced with PYTHIA 8.212 [44] to model the parton showering and fragmentation, as well as the decay of the τ leptons. The set of parton distribution functions (PDFs) is NNPDF3.0 [45]. The PYTHIA parameters affecting the description of the underlying event are set to the CUETP8M1 tune [46].

The generated events are processed through a simulation of the CMS detector based on GEANT4 [47], and are reconstructed with the same algorithms that are used for data. The simulated samples include additional pp interactions per bunch crossing, referred to as in-time pileup. Additionally the effect of inelastic collisions happening in the preceding and subsequent bunch crossings (out-of-time pileup) is considered. The effect of pileup is taken into account by generating concurrent minimum-bias collision events. The simulated events are weighted such that the distribution of the number of additional pileup interactions matches closely with data. The pileup distribution in data is estimated from the measured instantaneous luminosity for each bunch crossing, resulting in an average of approximately 23 interactions per bunch crossing.

4 Event reconstruction

Both observed and simulated events are reconstructed using the particle-flow (PF) algorithm [48]. The algorithm identifies and reconstructs the particles produced in pp collisions by combining information from all subdetectors. These so-called PF objects include photons, electrons, muons, neutral hadrons, and charged hadrons.

Any higher-level objects are reconstructed from combinations of the PF objects. For example, jets are reconstructed with an anti-k_T clustering algorithm implemented in the FASTJET library [49, 50]. The reconstruction is based on the clustering of neutral and charged PF objects with a distance parameter of 0.4. Additionally, charged PF objects are required to be associated with the primary vertex of the interaction.

While neutrinos cannot be detected directly, they contribute to missing transverse momentum. The missing transverse momentum vector $\vec{p}_T^{\,miss}$ is computed as the negative vector sum of the transverse momenta of all the PF objects in an event, and its magnitude is denoted as p_T^{miss} [51]. The $\vec{p}_T^{\,miss}$ is modified to account for corrections to the energy scale of the reconstructed jets in the event.

The primary pp interaction vertex is taken to be the reconstructed vertex with the largest value of summed p_T^2 of jets and the associated p_T^{miss}. In vertex reconstruction, the tracks assigned to each vertex are clustered into jets using the jet finding algorithm from Refs. [49, 52] and the associated transverse momentum is taken as the negative vector sum of the $\vec{p}_T$ of these jets.

Electrons are identified by a multivariate analysis (MVA) discriminant [53] that requires as

input several quantities describing the track quality, the shapes of the energy deposits in the ECAL, and the compatibility of the measurements from the tracker and the ECAL [54]. Muon identification relies on the number of measurements in the inner tracker and the muon systems, and on the quality of the reconstructed tracks [55]. Electrons and muons selected in this analysis are required to be consistent with originating from the primary vertex.

A lepton isolation discriminant I^{ℓ} is defined to reject nonprompt or misidentified leptons:

$$I^{\ell} \equiv \frac{\sum_{\text{charged}} p_{\text{T}} + \max\left(0, \sum_{\text{neutral}} p_{\text{T}} - \frac{1}{2}\sum_{\text{charged, PU}} p_{\text{T}}\right)}{p_{\text{T}}^{\ell}}, \tag{1}$$

where p_{T}^{ℓ} stands for the p_{T} of the lepton. The variable $\sum_{\text{charged}} p_{\text{T}}$ is the scalar sum of the transverse momenta of the charged particles originating from the primary vertex and located in a cone of size $\Delta R = \sqrt{(\Delta\eta)^2 + (\Delta\phi)^2} = 0.3\,(0.4)$ centered on the electron (muon) direction, where ϕ is the azimuthal angle in radians. The sum $\sum_{\text{neutral}} p_{\text{T}}$ represents a similar quantity for neutral particles. The scalar sum of the transverse momenta of charged hadrons in the cone originating from pileup vertices, $\sum_{\text{charged, PU}} p_{\text{T}}$, is used to estimate the contribution of photons and neutral hadrons originating from pileup vertices. The factor of $1/2$ corresponds approximately to the ratio of neutral to charged hadron production in the hadronization process of inelastic pp collisions, as estimated from simulation. The isolation requirements based on I^{ℓ} are described in the following section.

The combined secondary vertex algorithm [56] is used to identify jets that are likely to have originated from a bottom quark ("b-tagged jets"). In this algorithm the secondary vertices associated with the jet and the track-based lifetime information are given as inputs to an MVA discriminant designed for b jet identification. Any differences in the b tagging efficiency between data and simulation are taken into account by applying a set of p_{T}-dependent correction factors to simulated events [56]. An identification efficiency for genuine b jets is approximately 70%, whereas the misidentification probability for light flavor or gluon jets is approximately 1%.

Anti-k_{T} jets seed the hadron-plus-strips algorithm [57–59] which is used to reconstruct hadronically decaying τ leptons. In addition to one or more charged hadrons, hadronic tau decay paths can contain one or more π^0 particles. These π^0 are reconstructed by clustering together electromagnetic deposits in the ECAL into "strips" in the η–ϕ plane. The strips are elongated in the ϕ direction to contain energy lost to Bremsstrahlung radiation. The algorithm reconstructs τ_{h} candidates based on the number of tracks and the number of strips representing the number of charged hadrons ("prongs") and the number of π^0 present in the decay. The τ_{h} candidates used in this analysis are reconstructed in three decay modes: 1-prong, 1-prong+π^0, and 3-prong. Additionally, the reconstructed τ_{h} must have a mass consistent with their reconstructed decay mode.

To suppress objects (jets and leptons) misidentified as τ_{h} candidates, an MVA discriminant [59] including calorimetric information, isolation sums, and lifetime information is used. A misidentification rate for quark- and gluon-initiated jets of less than 1% is achieved within a p_{T} range typical of a τ_{h} originating from a h boson. Simultaneously, an efficiency for selecting τ_{h} candidates of about 65% is maintained for τ_{h} candidates passing the decay mode reconstruction discussed above. To suppress electrons and muons misidentified as τ_{h} candidates, dedicated criteria based on the consistency between the measurements in the tracker, the calorimeters, and the muon detectors are applied [57–59]. The τ_{h} energy scale is measured from $\text{Z} \to \tau\tau$ events and the correction is propagated to simulation for each decay mode. A "tag-and-probe"

measurement [60] in $Z \to \ell\ell$ events is used to correct the energy scale of electrons and muons misidentified as τ_h candidates in simulation.

The reconstructed mass of the A boson candidate can be used to discriminate between signal-like events and background-like events. Multiple reconstruction methods are considered. The simplest reconstructed mass, $m^{vis}_{\ell\ell\tau\tau}$, uses only the visible decay products and combines the reconstructed $Z \to \ell\ell$ four-vector with the $h \to \tau\tau$ four-vector based only on visible tau decay products. The resulting mass resolution for $m^{vis}_{\ell\ell\tau\tau}$ is approximately 15% for an A boson with mass 300 GeV in all final states.

The resolution of the reconstructed A boson candidate can be significantly improved by including information from the neutrinos associated with the leptonic and hadronic tau decays. To account for the neutrinos in the final states, the SVFIT algorithm is used to estimate the mass of the SM-like h boson, denoted as $m^{fit}_{\tau\tau}$. The SVFIT algorithm combines the $\vec{p}_T^{\,miss}$ with the four-vectors of both τ candidates, resulting in an estimate of the four-vector of the SM-like h boson that can be used to obtain a more accurate estimate of the A boson candidate mass $m^{fit}_{\ell\ell\tau\tau}$. The mass resolution of $m^{fit}_{\ell\ell\tau\tau}$ is 10% at 300 GeV.

To further increase the mass resolution, the known mass of the SM-like Higgs boson can be given as an input to the SVFIT algorithm. This yields a constrained estimate of the four-vector of the SM-like h boson and thus a constrained estimate of its mass $m^{c}_{\tau\tau}$. Using the constrained estimate of the four-vector of the SM-like h boson, we obtain an even more precise estimate of the A boson candidate mass, denoted as $m^{c}_{\ell\ell\tau\tau}$. The resulting mass resolution of $m^{c}_{\ell\ell\tau\tau}$ is as low as 3% at 300 GeV, which improves the expected 95% confidence level (CL) model-independent limits by approximately 40% compared to using the visible mass of the A boson $m^{vis}_{\ell\ell\tau\tau}$ as the discriminating variable. Thus, we use $m^{c}_{\ell\ell\tau\tau}$ as the discriminating variable between the signal and the background processes for the final results.

5 Event selection

Events are selected using single- or double-lepton triggers targeting leptonic decays of the Z bosons. The trigger and offline selection requirements for all possible decay modes are presented in Table 1. Leptons geometrically matched to the trigger-level leptons must be identified as the same ones which are selected in the analysis. The light leptons, i.e. electrons and muons, in the events are required to be separated from each other by $\Delta R > 0.3$, while the τ_h candidates must be separated from each other and from any other lepton by $\Delta R > 0.5$. The resulting event samples are made mutually exclusive by discarding events that have additional identified and isolated electrons or muons. Differences in trigger selection efficiencies are observed between data and simulation. These differences are accounted for by applying corrections to simulated events.

The non-triggering electrons and muons are required to have $p_T > 10$ GeV, whereas τ_h candidates must have $p_T > 20$ GeV. The $|\eta|$ constraints from detectory geometry are $|\eta|^e < 2.5$, $|\eta|^\mu < 2.4$, and $|\eta|^{\tau_h} < 2.3$ for electrons, muons, and τ_h candidates, respectively. The $|\eta|$ thresholds are the same for both triggering and non-triggering electrons and muons.

The Z boson is reconstructed from the opposite charge, same-flavor light lepton combination that fulfills $60 < m_{\ell\ell} < 120$ GeV. In case of multiple Z boson candidates, we choose the one with a mass closest to the Z boson mass. Looser identification and isolation selection criteria are applied to the leptons associated to the Z boson to maintain a high signal acceptance. The electrons (muons) associated to a Z boson decay must pass the identification with 90% (> 99%)

efficiency. The muons must pass an additional isolation requirement of $I^{\mu} < 0.25$.

The leptons associated to the SM-like Higgs boson are required to have opposite charge. Tighter selection criteria are applied to the two light leptons forming the SM-like Higgs boson candidate to decrease the background contributions from Z + jets and other reducible backgrounds. The specific signal selections detailed in Table 2, including those chosen for the τ_h candidates, were optimized to obtain the best signal sensitivity. The isolation requirements are $I^{e} < 0.15$ ($I^{\mu} < 0.15$) for electrons (muons) associated to a τ_h decay. Electrons from a τ_h decay need to pass electron identification with 80% efficiency. All τ_h candidates must satisfy τ_h identification and isolation with 95% efficiency, but for the τ_h candidates associated with the SM-like Higgs boson, tighter identification and isolation requirements corresponding to 65% efficiency are applied.

As the signal events contain no b jets (ggA), or only b jets with relatively soft p_T distribution (bbA), we can suppress the contributions of $t\bar{t}$ and $t\bar{t}Z$ by discarding all events with one or more b-tagged jets ("b jet veto") without significantly reducing the signal selection efficiency.

The sensitivity of the analysis can be improved by reducing the amount of background events using additional information regarding the SM-like Higgs boson candidate. The constrained Higgs boson candidate four-vector, as estimated with SVFIT algorithm, is already used to reconstruct the A boson mass as described in Section 4. As the shape of the constrained estimate of the h boson mass $m^{c}_{\tau\tau}$ distribution is similar for the signal and background events, we do not gain sensitivity by selecting events based on values of this variable. By removing the mass constraint from the SVFIT algorithm, the most likely mass of the SM-like Higgs boson candidate $m^{fit}_{\tau\tau}$ provides significant discrimination between reducible backgrounds, which have a broad distribution due to their lack of a resonance, and the signal processes which have a resonance at 125 GeV. Additionally, the dominant irreducible background ZZ is suppressed because of its softer distribution compared to the signal processes. The sensitivity is increased by an additional 20% by requiring $m^{fit}_{\tau\tau}$ to be within 90–180 GeV.

The large h boson mass leads to relatively high-p_T decay products compared to the lower p_T of the jets misidentified as leptons from the Z + jets background process. In the $\ell\ell + \tau_h\tau_h$ final states, which have a larger relative fraction of reducible-to-irreducible backgrounds, the expected signal sensitivity is increased by selecting events based on the scalar p_T sum of the visible decay products of the SM-like Higgs boson, L^{h}_{T}. Events are selected with $L^{h}_{T} > 60$ GeV.

Table 1: Trigger and offline selection requirements for Z boson decay modes. The events are selected with either a lower-p_T threshold double lepton trigger or a higher-p_T threshold single lepton trigger. The subscripts 1 and 2 stand for the higher-p_T and lower-p_T leptons associated with the Z boson, respectively.

Decay channel	$Z \to \ell\ell$ trigger selection	$Z \to \ell\ell$ offline selection
$Z \to ee$	$\left[p_T^{e_1} > 23\,\text{GeV}\ \&\ p_T^{e_2} > 12\,\text{GeV}\right]$ or $p_T^{e_1} > 27\,\text{GeV}$	$\left[p_T^{e_1} > 24\,\text{GeV}\ \&\ p_T^{e_2} > 13\,\text{GeV}\right]$ or $p_T^{e_1} > 28\,\text{GeV}$
$Z \to \mu\mu$	$\left[p_T^{\mu_1} > 17\,\text{GeV}\ \&\ p_T^{\mu_2} > 8\,\text{GeV}\right]$ or $p_T^{\mu_1} > 24\,\text{GeV}$	$\left[p_T^{\mu_1} > 18\,\text{GeV}\ \&\ p_T^{\mu_2} > 10\,\text{GeV}\right]$ or $p_T^{\mu_1} > 25\,\text{GeV}$

6 Background estimation

The irreducible backgrounds (ZZ, $t\bar{t}Z$, WWZ, WZZ, ZZZ) are estimated from simulation and scaled by their theoretical cross sections at the highest order available. The production of the 125 GeV Higgs boson via the processes predicted by the SM are also estimated from simulation

Table 2: Kinematic selection requirements for each A boson channel, applied on top of the looser selections and b jet veto described in text, with the exception that muons associated to the Z boson must also pass the identification requirement with $> 99\%$ efficiency. The identification (and isolation) requirements are described by $\epsilon^{\ell}_{\text{id.}}$ that stands for efficiency for given lepton type. The leptons assigned to the SM-like Higgs boson are required to have opposite charge. To increase the sensitivity, we require $m^{\text{fit}}_{\tau\tau}$ to be within 90–180 GeV. In the $\ell\ell + \tau_{\text{h}}\tau_{\text{h}}$ channel we additionally require $L^{\text{h}}_{\text{T}} > 60\,\text{GeV}$.

Channel	Z boson selection	h boson selection
$\ell\ell + \mu\tau_{\text{h}}$	Opposite charge, same-flavor light leptons $60 < m_{\ell\ell} < 120\,\text{GeV}$	$\epsilon^{\mu}_{\text{id.}} > 99\%$, $I^{\mu} < 0.15$
$\ell\ell + \text{e}\tau_{\text{h}}$		$\epsilon^{\text{e}}_{\text{id.}} = 80\%$, $I^{\text{e}} < 0.15$, $\epsilon^{\tau_{\text{h}}}_{\text{id.+iso.}} = 65\%$
$\ell\ell + \tau_{\text{h}}\tau_{\text{h}}$		$\epsilon^{\tau_{\text{h}}}_{\text{id.+iso.}} = 65\%$
$\ell\ell + \text{e}\mu$		$\epsilon^{\text{e}}_{\text{id.}} = 80\%$, $I^{\text{e}} < 0.15$, $\epsilon^{\mu}_{\text{id.}} > 99\%$, $I^{\mu} < 0.15$

and are scaled to the theoretical cross sections at the highest order available and by their most accurate branching fractions [38].

The reducible backgrounds, which have at least one jet misidentified as an electron, muon, or τ_{h} candidate, are estimated from data. The dominant reducible contributions come from $\text{t}\bar{\text{t}}$, $\text{Z} + \text{jets}$, and $\text{WZ} + \text{jets}$ processes. The estimation of the reducible background contribution is performed with so called "fake rate method" which is based on measuring the misidentification rates, i.e. probabilities to misidentify a jet as a lepton. Events with τ candidates (electrons, muons, or τ_{h}) failing the signal region identification and isolation criteria are used along with the misidentification rates to estimate the contribution of processes with jets misidentified as τ candidates in the signal region.

The misidentification rates are estimated in event samples independent from the signal region. In this analysis we use a sample of $\text{Z} + \text{jet}$ events. The misidentification rates are measured in different bins of lepton p_{T}, and are further split between reconstructed decay modes for the τ_{h} candidate and for muons and electrons in bins of lepton η based on barrel and endcap regions. The measured misidentification rates are validated in an orthogonal region that consists of events with a Z candidate and 2 jets. To ensure the validation is not contaminated with signal events or significant irreducible background contributions, the two lepton candidates associated with the Higgs boson are required to have the same charge.

The estimation of misidentification rates relies on reconstructing an opposite charge same-flavor lepton pair compatible with a Z boson, and requiring one additional loosely defined lepton (electron, muon, or τ_{h} candidate). The requirements on the leptons associated to the Z boson are the same as defined in Section 5, but they must fulfill a more stringent Z mass requirement, $81.2 < m_{\ell\ell} < 120\,\text{GeV}$. After reconstructing the $\text{Z} \to \ell\ell$ decay, the jet-to-lepton misidentification rate is estimated by applying the lepton identification algorithm to the additional loosely defined lepton in the event. The events where the τ candidates arise from genuine leptons and not jets, primarily from the WZ process, are estimated from simulation and subtracted from the data so that the misidentification rates are measured for jets only.

To estimate the reducible background contribution in the signal region, we apply a weight on data events where either one or both of the τ candidates associated to the SM-like Higgs boson fail the identification and isolation criteria. Events with exactly one object failing the identification and isolation criteria receive a weight $f/(1-f)$, where f is the misidentification rate for the particular type of lepton. As such, this weight includes the contribution from the $\text{WZ} + \text{jets}$ process, where we expect one real lepton and one jet misidentified as a lepton in addition to the Z boson candidate. Also $\text{t}\bar{\text{t}}$ and $\text{Z} + \text{jets}$ processes are accounted for by the weight as either of the two jets can pass the identification and isolation criteria even if neither

of them are real leptons. As a result, the weight introduces double counting of events from $\mathrm{t\bar{t}}$ and $\mathrm{Z}+$jets processes that should have both candidates failing the selection criteria.

To remove the double-counted events from $\mathrm{t\bar{t}}$ and $\mathrm{Z}+$jets processes, we define a weight with a negative sign that is given for events with both objects failing the identification and isolation criteria, namely $-f_1 f_2/[(1-f_1)(1-f_2)]$. This subtraction, however, introduces increased statistical uncertainties on the estimated yield of the reducible background. The statistical uncertainties can be controlled by taking the shape of the $m^{\mathrm{c}}_{\ell\ell\tau\tau}$ distribution of the reducible background contribution from data in a region with negligible signal and irreducible background contributions, defined similarly to the signal region but with same-sign τ candidates passing relaxed identification and isolation criteria. This results in a smoother shape of the $m^{\mathrm{c}}_{\ell\ell\tau\tau}$ distribution.

Instead of using the same-sign data events for the shape of the $m^{\mathrm{c}}_{\ell\ell\tau\tau}$ distribution, the statistical uncertainties can alternatively be reduced considerably by giving a suitable nonzero weight only for events with both candidates failing the selection criteria, i.e. by estimating only the contribution from the $\mathrm{t\bar{t}}$ and $\mathrm{Z}+$jets processes by using the fake rate method. This alternative approach offers a cross-check against the nominal method and requires some changes such as predicting the contribution from events with a single object failing the identification and isolation criteria from simulation and using a weight with a positive sign ($f_1 f_2/[(1-f_1)(1-f_2)]$) because there is no double counting in contrast to the nominal method. The shape of the $m^{\mathrm{c}}_{\ell\ell\tau\tau}$ distribution is taken from the same events that provide the estimated yield of the reducible background. The results of the cross check show the two methods yield consistent expected 95% CL model-independent limits.

To cross check the measured misidentification rates, we performed an additional measurement using a sample of $\mathrm{Z}+2$ jets events. In this cross check the measurement region partially overlaps with the aforementioned validation region, as in both cases the two lepton candidates associated with the Higgs boson are required to have the same charge. The amount of overlap between the measurement and validation regions depends on the lepton type and the decay channel of the Higgs boson. The rates are measured in bins of lepton p_{T}, and are separated by the reconstructed decay mode of the τ_{h} candidates. Unlike above, the misidentification rates are not split in bins of lepton η for muons and electrons. The measured misidentification rates result in a reducible background yield and shape that are compatible with the reducible background estimation obtained with the nominal misidentification rate measurement used in this analysis.

7 Systematic uncertainties

All systematic uncertainties considered in the analysis are summarized in Table 3. Different uncertainties are treated as uncorrelated, and each uncertainty is correlated between different processes and final states, unless otherwise mentioned below.

The overall uncertainty in the τ_{h} identification and isolation efficiency for genuine τ_{h} leptons is 5% [58], which has been measured with a tag-and-probe method in $\mathrm{Z}\to\tau\tau$ events. An uncertainty of 1.2% in the visible energy (neutrino component excluded) scale of genuine τ_{h} affects both the distributions and yields of the signals and backgrounds. It is uncorrelated among the 1-prong, 1-prong+π^0, and 3-prong decay modes.

The uncertainties in the electron and muon identification and isolation efficiencies lead to a normalization uncertainty of 2% for both electrons and muons. The uncertainty in the trigger

efficiency results in a normalization uncertainty of 2% for the electron triggers and 2% for the muon triggers. In all channels, the effect of the uncertainty in the muon and electron energy scales is negligible.

The normalization uncertainty related to discarding events with a b-tagged jet is 4.5% for processes with heavy-flavor jets, and 0.15% for processes with light-flavor jets.

The normalization uncertainties related to the choice of the PDFs and the QCD renormalization and factorization scales, affecting the acceptance of the dominant background processes, are estimated from simulation separately for each process. They cover the uncertainties in the parton shower modeling. The uncertainty from the renormalization and factorization scales is determined by varying these scales independently by factors of 0.5 and 2.0, and calculating the change in process acceptance. Combining the renormalization and factorization scale uncertainties with the PDF set uncertainty [61] for the $qq \to ZZ$ process leads to an uncertainty of 4.8%. The inclusive uncertainty for the Zh production related to the PDFs amounts to 1.6%, whereas the uncertainty for the variation of the renormalization and factorization scales is 3.8% [38]. For the subleading Higgs boson processes Wh, $gg \to ZZ$, and $t\bar{t}h$ the inclusive uncertainties related to the PDFs amount to 1.9, 3.2, and 3.6% and the uncertainties for the variation of the renormalization and factorization scales are 0.7, 3.9, and 7.5%, respectively [38].

For the $gg \to ZZ$ process, there is a 10% uncertainty in the NLO K factor used in the analysis which is dominant compared to PDF and QCD renormalization and factorization scale uncertainties. The uncertainties in the cross section of the rare $t\bar{t}Z$, $t\bar{t}W$, and triboson processes amount to 25% [62], which dominates other theoretical uncertainties for these processes.

The final theoretical uncertainty applied in this analysis is the uncertainty in the theoretical calculations of the SM $h \to \tau\tau$ branching fraction. This uncertainty of 2% is applied to both the ggA and bbA signal samples as well as all backgrounds that include the $h \to \tau\tau$ process.

Normalization uncertainties in the misidentification rates arising from the subtraction of prompt leptons estimated from simulation are taken into account and propagated to the yield of the reducible background mass distributions. The shape of the mass distribution of the reducible background is estimated from data in a region where the τ candidates have the same charge and pass relaxed isolation conditions. Therefore, the statistical uncertainties in the misidentification rates do not have an impact on the shape of the mass distribution. An additional uncertainty is applied based on potential differences between the region where the misidentification rates are measured and the region where they are applied. These uncertainties are based on the results of closure tests comparing the differences in observed versus predicted reducible background yields. The uncertainty in the yield is taken to be 40%, conservative enough to cover the observed non-closure, and is uncorrelated between the SM-like Higgs boson decay channels resulting in 4 uncertainties tied to $\ell\ell + \mu\tau_h$, $\ell\ell + e\tau_h$, $\ell\ell + \tau_h\tau_h$, and $\ell\ell + e\mu$ channels.

The $\vec{p}_T^{\,miss}$ scale uncertainties [63], which are computed event-by-event, affect the normalization of various processes as well as their distributions through the propagation of these uncertainties to the di-τ masses $m_{\tau\tau}^{fit}$ and $m_{\tau\tau}^{c}$. The $\vec{p}_T^{\,miss}$ scale uncertainties arising from unclustered energy deposits in the detector come from four independent sources related to the tracker, ECAL, the hadron calorimeter, and forward calorimeters. Additionally, $\vec{p}_T^{\,miss}$ scale uncertainties related to the uncertainties in the jet energy scale measurement, which affect the $\vec{p}_T^{\,miss}$ calculation, are taken into account.

Uncertainties related to the finite number of simulated events are taken into account. They are considered for all bins of the signal and background distributions used to extract the results. They are uncorrelated across different samples, and across bins of a single distribution. Finally,

the uncertainty in the integrated luminosity amounts to 2.5% [64].

Table 3: Sources of systematic uncertainty. The sign † marks the uncertainties that affect both the shape and normalization of the final $m^{c}_{\ell\ell\tau\tau}$ distributions. Uncertainties that only affect the normalizations have no marker. For the shape and normalization uncertainties, the magnitude column lists an approximation of the associated change in normalization.

Source of uncertainty	Magnitude	Process
τ_h id. & isolation	5%	All simulations
τ_h energy scale† (1.2% energy shift)	<2%	All simulations
e id. & isolation	2%	All simulations
e trigger	2%	All simulations
μ id. & isolation	2%	All simulations
μ trigger	2%	All simulations
b jet veto	4.5% heavy flavor, 0.15% light flavor	All simulations
$qq \to ZZ$ theoretical uncertainty	4.8%	$qq \to ZZ$
$gg \to ZZ$ NLO K factor	10%	$gg \to ZZ$
$t\bar{t}Z$ theoretical uncertainty	25%	$t\bar{t}Z$
$t\bar{t}W$ theoretical uncertainty	25%	$t\bar{t}W$
triboson theoretical uncertainty	25%	triboson
Theoretical uncertainty on $\mathcal{B}(h \to \tau\tau)$	<2%	Signal, Zh, and Wh
Reducible background uncertainties:		Reducible background
e prompt lepton subtraction	<12% in $\ell\ell + e\mu$, <1% in $\ell\ell + e\tau_h$	
μ prompt lepton subtraction	<16% in $\ell\ell + e\mu$, <1.5% in $\ell\ell + \mu\tau_h$	
τ prompt lepton subtraction	<3.5% in $\ell\ell + e\tau_h$ and $\ell\ell + \mu\tau_h$, <1% in $\ell\ell + \tau_h\tau_h$	
normalization	40% in $\ell\ell + e\tau_h$, $\ell\ell + \mu\tau_h$, $\ell\ell + \tau_h\tau_h$, and $\ell\ell + e\mu$	
$\vec{p}_T^{\,miss}$ energy scale†	<2%	All simulations
Limited number of events	Statistical uncertainty in individual bins	All background processes
Integrated luminosity	2.5%	All simulations

8 Results

The analysis sets 95% CL upper limits [65, 66] in multiple scenarios. Model-independent limits are set on the product of the cross section and branching fraction, $\sigma(ggA)\,\mathcal{B}(A \to Zh \to \ell\ell\tau\tau)$, for the $ggA \to Zh$ process. Model-dependent limits are set for two MSSM benchmark scenarios. An asymptotic approximation [67, 68] is used when calculating the 95% CL upper limits. The limits are based on a simultaneous fit of the reconstructed pseudoscalar Higgs boson mass distributions in the eight signal regions. We use the reconstructed mass, $m^{c}_{\ell\ell\tau\tau}$, as the discriminating variable between the signal and the background processes. Even though the studied signal mass range is 220–400 GeV, the distribution of the reconstructed mass $m^{c}_{\ell\ell\tau\tau}$ covers mass range 200–600 GeV as the additional information on the background distributions is used to constrain the simultaneous fit.

The eight final states are each fit as separate distributions in the simultaneous fit. They are combined together for visualization purposes only. When displaying the results, background processes are grouped as follows: "Production of a 125 GeV h boson" includes all processes with the SM Higgs boson (including $ggh \to ZZ \to 4l$), "$ZZ \to 4l$ (excl. $h \to ZZ \to 4l$)" includes all events except $ggh \to ZZ \to 4l$, "Other" includes events from triboson, $t\bar{t}Z$ and $t\bar{t}W$ production, and "Reducible" includes the reducible background contribution.

The $m^{c}_{\ell\ell\tau\tau}$ distributions are shown in Fig. 1 for each of the four Zh channels, and in Fig. 2 for all eight final states together. The distributions are shown after a background-only fit and include both statistical and systematic uncertainties. The signal and background predicted yields, as well as the number of observed events, are given for each of the four Zh channels in Table 4.

The model-independent 95% CL limits are shown in Fig. 3 and are in agreement with the SM prediction. In addition, multiple MSSM scenarios are considered where 95% CL limits are set

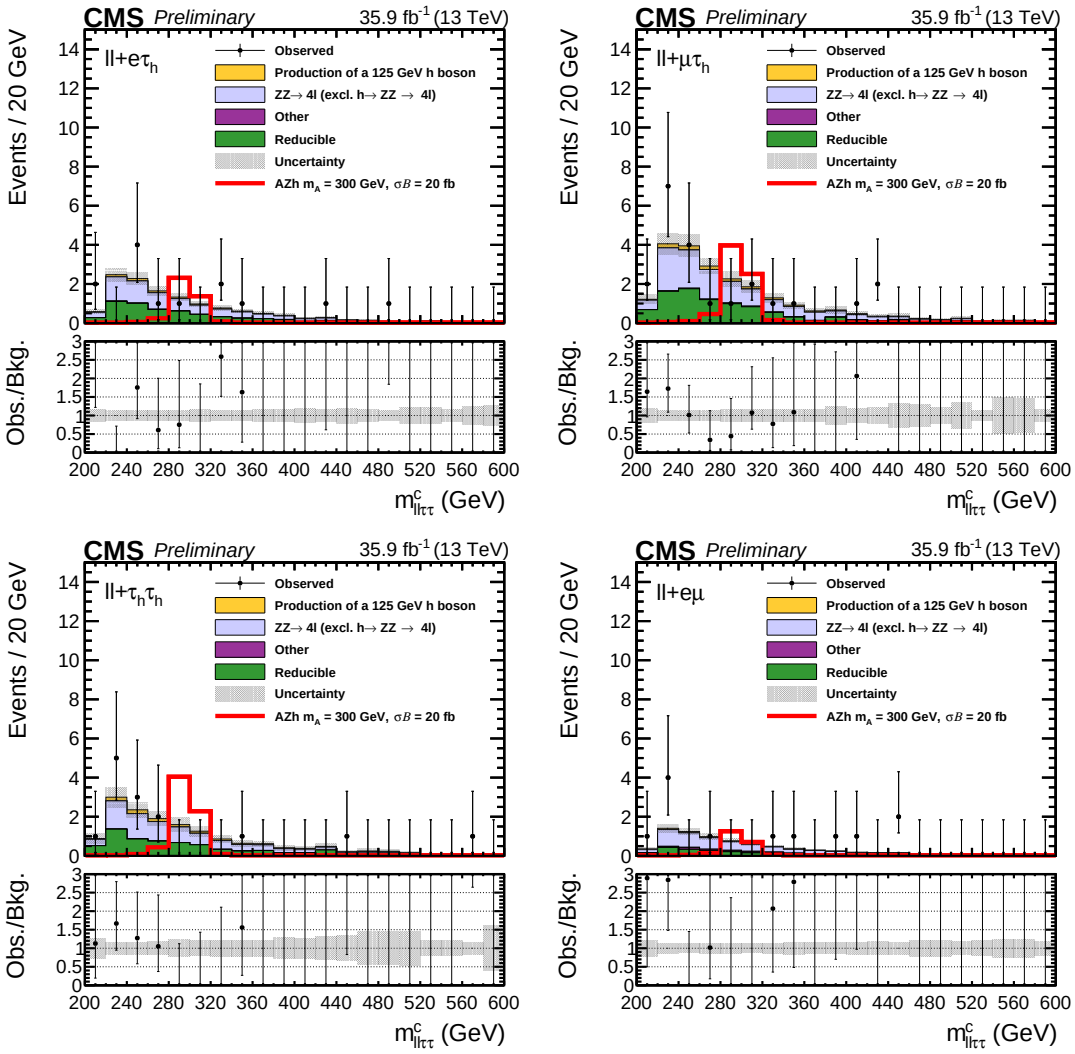

Figure 1: Reconstructed mass $m^{c}_{\ell\ell\tau\tau}$ distributions and uncertainties after a background-only fit for (upper left) $\ell\ell + e\tau_h$, (upper right) $\ell\ell + \mu\tau_h$, (lower left) $\ell\ell + \tau_h\tau_h$, and (lower right) $\ell\ell + e\mu$. In all cases the two decay channels of the Z boson are each included as separate distributions in the simultaneous fit; combining them together is for visualization purposes only. The uncertainties include both statistical and systematic components. The contribution from the AZh yields are the numbers of expected signal events for a pseudoscalar Higgs boson with $m_A = 300\,\text{GeV}$ with the product of the cross section and branching fraction of 20 fb and is for illustration only.

in the m_A–tan β plane. The Low tan β scenario and the hMSSM scenario are shown in Fig. 4. The previous observed (expected) limits by the CMS Collaboration [23] excluded the m_A–tan β plane to tan $\beta = 2.7$ (2.4) at $m_A = 300\,\text{GeV}$ in the Low tan β scenario, whereas tan β value of 3.8 (3.2) is reached by this analysis. Thus, the limits are improved by more than 30% for $m_A = 300\,\text{GeV}$. The improvement in the limits is mainly due to the new mass reconstruction method described in Section 4, and the amount of improvement depends on the mass point.

For both scenarios limits are set based on the ggA and bbA pseudoscalar A production processes. The signal samples used in the analysis are generated with the ggA process. To account for the bbA production, at each point in the m_A–tan β plane, the yield of the signal process

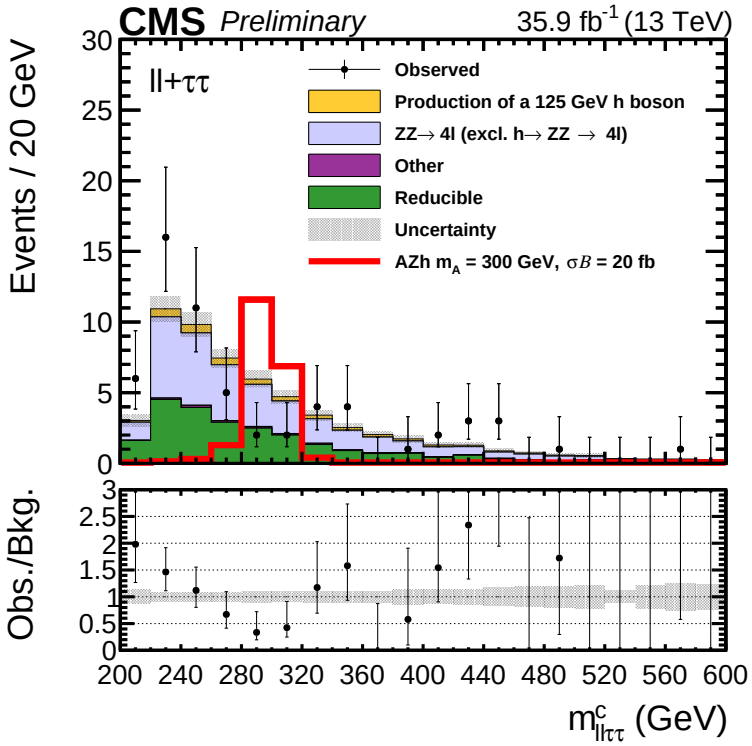

Figure 2: Reconstructed mass $m^{c}_{\ell\ell\tau\tau}$ distribution and uncertainties after a background-only fit in all eight final states. The final states are each included as separate distributions in the simultaneous fit; combining them together is for visualization purposes only. The uncertainties include both statistical and systematic components. The contribution from the AZh yield is the number of expected signal events for a pseudoscalar Higgs boson with $m_{\mathrm{A}} = 300\,\mathrm{GeV}$ with the product of the cross section and branching fraction of 20 fb and is for illustration only.

resulting from ggA is scaled according to Eq. (2) to account for the bbA contribution:

$$\text{Total signal yield} = \text{ggA yield} \times \left(1 + \epsilon_{\mathrm{bbA/ggA}} \times \frac{\sigma_{\mathrm{bbA}}}{\sigma_{\mathrm{ggA}}}\right). \tag{2}$$

The scaling takes the estimated ggA yield at each grid point and adds a contribution associated to bbA according to the measured difference in the signal region selection efficiency, $\epsilon_{\mathrm{bbA/ggA}} = 0.76$, and the ratio $\sigma_{\mathrm{bbA}}/\sigma_{\mathrm{ggA}}$, which depends on m_{A} and $\tan\beta$. The signal yield scaling allows us to include the estimated bbA contribution which is necessary when setting model-dependent limits in phase space region where the bbA cross section becomes non-negligible compared to the ggA cross section. For reference, at $m_{\mathrm{A}} = 300\,\mathrm{GeV}$ and $\tan\beta = 4$, in the hMSSM scenario, $\sigma_{\mathrm{bbA}}/\sigma_{\mathrm{ggA}} = 0.22$, which is a non-negligible contribution. In the Low $\tan\beta$ scenario, Higgs boson masses and mixing (and effective Yukawa couplings) have been calculated with FeynHiggs [69–73]. For the gluon-fusion process inclusive cross sections are obtained with SusHi [74], which includes NLO supersymmetric-QCD corrections [75–80], next-to-NLO QCD corrections for the top-quark contribution in the effective theory of a heavy top quark [81–85] and electroweak effects by light quarks [86, 87]. Five-flavour next-to-NLO QCD inclusive cross sections are calculated with SusHi [74] based on bbh@nnlo [88]. The results are combined with the four-flavour NLO QCD calculation [89, 90]. Whereas in the hMSSM branching ratios are solely computed with HDECAY [91, 92], the Low $\tan\beta$ scenario combines the most precise results of HDECAY, FeynHiggs and PROPHECY4f [93–95].

Table 4: Background and signal expectations together with the numbers of observed events, for the signal region distributions after a background-only fit. The AZh yields are the numbers of expected signal events for a pseudoscalar Higgs boson with $m_A = 300\,\text{GeV}$ with the product of the cross section and branching fraction of 20 fb. The background uncertainty accounts for all sources of background uncertainty, systematic as well as statistical, after the simultaneous fit.

Process	$\ell\ell + e\tau_h$	$\ell\ell + \mu\tau_h$	$\ell\ell + \tau_h\tau_h$	$\ell\ell + e\mu$
Production of a 125 GeV h boson	0.77 ± 0.02	1.39 ± 0.03	1.28 ± 0.04	0.45 ± 0.01
ZZ $\rightarrow$ 4l (excl. h $\rightarrow$ ZZ $\rightarrow$ 4l)	6.48 ± 0.14	11.37 ± 0.24	7.58 ± 0.20	4.56 ± 0.09
Other	0.10 ± 0.01	0.24 ± 0.02	0.04 ± 0.01	0.69 ± 0.04
Reducible	5.52 ± 0.47	9.12 ± 0.85	6.68 ± 0.70	2.04 ± 0.23
Total background	12.87 ± 0.50	22.12 ± 0.87	15.58 ± 0.76	7.74 ± 0.27
AZh, $m_A = 300\,\text{GeV}$, $\sigma\mathcal{B} = 20$ fb	4.13 ± 0.18	7.32 ± 0.30	7.01 ± 0.40	2.26 ± 0.10
Observed	13	22	14	12

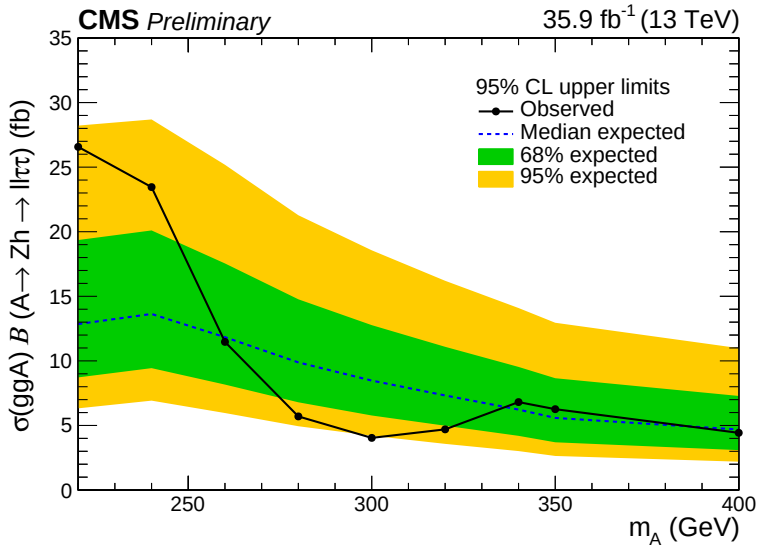

Figure 3: The expected and observed 95% CL model-independent limits are shown for the product of the cross section and branching fraction for the studied process: $\sigma\,(\text{ggA})\,\mathcal{B}\,(\text{A} \rightarrow \text{Zh} \rightarrow \ell\ell\tau\tau)$. The green (yellow) bands correspond to the 68% (95%) confidence intervals for the expected limit.

9 Summary

A search is presented for a pseudoscalar Higgs boson decaying into a standard model-like Higgs boson that further decays into tau leptons and a leptonically decaying Z boson. A data sample of proton-proton collisions collected at $\sqrt{s} = 13\,\text{TeV}$ by the CMS experiment at the LHC is used, and corresponds to an integrated luminosity of $35.9\,\text{fb}^{-1}$. The sensitivity of the study is increased by using the information on the standard model-like Higgs boson mass from the previous mass measurements when reconstructing the mass of the pseudoscalar Higgs boson. The signal extraction is further optimized with kinematic selections based on the mass of the standard model-like Higgs boson. In the absence of observing the signal, model-independent limits are set. Model-dependent exclusion limits are set in the m_A–$\tan\beta$ plane for two distinct Minimal supersymmetric standard model scenarios, Low $\tan\beta$ and hMSSM. This analysis brings complementary sensitivity to analyses excluding m_A–$\tan\beta$ phase space at high $\tan\beta$ values by adding exclusion power at low $\tan\beta$ values.

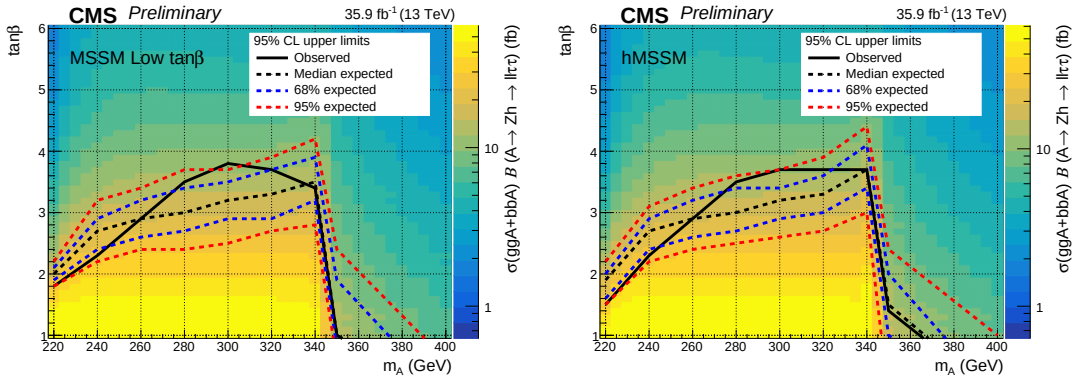

Figure 4: The expected and observed 95% CL exclusion limits in the m_{A}–tan β plane are shown for two MSSM scenarios: (left) Low tan β and (right) hMSSM. The excluded region is the lower m_{A} and lower tan β phase space. The limits are overlaid on a background showing the theorized $\sigma\,(\mathrm{ggA} + \mathrm{bbA})\,\mathcal{B}\,(\mathrm{A} \to \mathrm{Zh} \to \ell\ell\tau\tau)$ at each grid point.

References

[1] S. Weinberg, "A model of leptons", *Phys. Rev. Lett.* **19** (1967) 1264, doi:10.1103/PhysRevLett.19.1264.

[2] A. Salam, "Weak and electromagnetic interactions", in *Elementary particle physics: relativistic groups and analyticity*, N. Svartholm, ed., p. 367. Almqvist & Wiksell, Stockholm, 1968. Proceedings of the eighth Nobel symposium.

[3] F. Englert and R. Brout, "Broken symmetry and the mass of gauge vector mesons", *Phys. Rev. Lett.* **13** (1964) 321, doi:10.1103/PhysRevLett.13.321.

[4] P. W. Higgs, "Broken symmetries, massless particles and gauge fields", *Phys. Lett.* **12** (1964) 132, doi:10.1016/0031-9163(64)91136-9.

[5] P. W. Higgs, "Broken symmetries and the masses of gauge bosons", *Phys. Rev. Lett.* **13** (1964) 508, doi:10.1103/PhysRevLett.13.508.

[6] G. S. Guralnik, C. R. Hagen, and T. W. B. Kibble, "Global conservation laws and massless particles", *Phys. Rev. Lett.* **13** (1964) 585, doi:10.1103/PhysRevLett.13.585.

[7] P. W. Higgs, "Spontaneous symmetry breakdown without massless bosons", *Phys. Rev.* **145** (1966) 1156, doi:10.1103/PhysRev.145.1156.

[8] T. W. B. Kibble, "Symmetry breaking in non-Abelian gauge theories", *Phys. Rev.* **155** (1967) 1554, doi:10.1103/PhysRev.155.1554.

[9] ATLAS Collaboration, "Observation of a new particle in the search for the standard model Higgs boson with the ATLAS detector at the LHC", *Phys. Lett. B* **716** (2012) 1, doi:10.1016/j.physletb.2012.08.020, arXiv:1207.7214.

[10] CMS Collaboration, "Observation of a new boson at a mass of 125 GeV with the CMS experiment at the LHC", *Phys. Lett. B* **716** (2012) 30, doi:10.1016/j.physletb.2012.08.021, arXiv:1207.7235.

[11] CMS Collaboration, "Observation of a new boson with mass near 125 GeV in pp collisions at $\sqrt{s}$ = 7 and 8 TeV", *JHEP* **06** (2013) 081, doi:10.1007/JHEP06(2013)081, arXiv:1303.4571.

[12] CMS Collaboration, "Measurements of properties of the Higgs boson decaying into the four-lepton final state in pp collisions at $\sqrt{s} = 13$ TeV", *JHEP* **11** (2017) 047, doi:10.1007/JHEP11(2017)047, arXiv:1706.09936.

[13] ATLAS and CMS Collaborations, "Combined measurement of the Higgs boson mass in pp collisions at $\sqrt{s} = 7$ and 8 TeV with the ATLAS and CMS experiments", *Phys. Rev. Lett.* **114** (2015) 191803, doi:10.1103/PhysRevLett.114.191803, arXiv:1503.07589.

[14] ATLAS Collaboration, "Measurement of the Higgs boson mass in the $H \to ZZ^* \to 4\ell$ and $H \to \gamma\gamma$ channels with $\sqrt{s} = 13$ TeV pp collisions using the ATLAS detector", (2018). arXiv:1806.00242. Submitted to *PLB*.

[15] ATLAS and CMS Collaborations, "Measurements of the Higgs boson production and decay rates and constraints on its couplings from a combined ATLAS and CMS analysis of the LHC pp collision data at $\sqrt{s} = 7$ and 8 TeV", *JHEP* **08** (2016) 045, doi:10.1007/JHEP08(2016)045, arXiv:1606.02266.

[16] CMS Collaboration, "Measurement and interpretation of differential cross sections for Higgs boson production at $\sqrt{s} = 13$ TeV", *Submitted to: Phys. Lett.* (2018) arXiv:1812.06504.

[17] T. D. Lee, "A theory of spontaneous T violation", *Phys. Rev. D* **8** (1973) 1226–1239, doi:10.1103/PhysRevD.8.1226.

[18] G. C. Branco et al., "Theory and phenomenology of two-Higgs-doublet models", *Phys. Rept.* **516** (2012) 1–102, doi:10.1016/j.physrep.2012.02.002, arXiv:1106.0034.

[19] E. Bagnaschi et al., "Benchmark scenarios for low tan β in the MSSM", Technical Report LHCHXSWG-2015-002, CERN, Geneva, 2015.

[20] A. Djouadi et al., "The post-Higgs MSSM scenario: Habemus MSSM?", *Eur. Phys. J. C* **73** (2013) 2650, doi:10.1140/epjc/s10052-013-2650-0, arXiv:1307.5205.

[21] M. Carena et al., "MSSM Higgs boson searches at the LHC: Benchmark scenarios after the discovery of a Higgs-like particle", *Eur. Phys. J. C* **73** (2013), no. 9, 2552, doi:10.1140/epjc/s10052-013-2552-1, arXiv:1302.7033.

[22] ATLAS Collaboration, "Search for a CP-odd Higgs boson decaying to Zh in pp collisions at $\sqrt{s} = 8$ TeV with the ATLAS detector", *Phys. Lett. B* **744** (2015) 163–183, doi:10.1016/j.physletb.2015.03.054, arXiv:1502.04478.

[23] CMS Collaboration, "Searches for a heavy scalar boson H decaying to a pair of 125 GeV Higgs bosons hh or for a heavy pseudoscalar boson A decaying to Zh, in the final states with $h \to \tau\tau$", *Phys. Lett. B* **755** (2016) 217–244, doi:10.1016/j.physletb.2016.01.056, arXiv:1510.01181.

[24] ATLAS Collaboration, "Search for heavy resonances decaying into a W or Z boson and a Higgs boson in final states with leptons and b-jets in 36 fb^{-1} of $\sqrt{s} = 13$ TeV pp collisions with the ATLAS detector", *JHEP* **03** (2018) 174, doi:10.1007/JHEP03(2018)174, arXiv:1712.06518. [Erratum: doi:10.1007/JHEP11(2018)051].

[25] CMS Collaboration, "Search for a heavy pseudoscalar boson decaying to a Z and a Higgs boson at $\sqrt{s} = 13$ TeV", arXiv:1903.00941. Submitted to *EPJC*.

[26] L. Bianchini, J. Conway, E. K. Friis, and C. Veelken, "Reconstruction of the Higgs mass in $H \to \tau\tau$ events by dynamical likelihood techniques", *J. Phys. Conf. Ser.* **513** (2014) 022035, doi:10.1088/1742-6596/513/2/022035.

[27] CMS Collaboration, "The CMS trigger system", *JINST* **12** (2017) P01020, doi:10.1088/1748-0221/12/01/P01020, arXiv:1609.02366.

[28] CMS Collaboration, "The CMS experiment at the CERN LHC", *JINST* **3** (2008) S08004, doi:10.1088/1748-0221/3/08/S08004.

[29] J. Alwall et al., "The automated computation of tree-level and next-to-leading order differential cross sections, and their matching to parton shower simulations", *JHEP* **07** (2014) 079, doi:10.1007/JHEP07(2014)079, arXiv:1405.0301.

[30] P. Nason, "A new method for combining NLO QCD with shower Monte Carlo algorithms", *JHEP* **11** (2004) 040, doi:10.1088/1126-6708/2004/11/040, arXiv:hep-ph/0409146.

[31] S. Frixione, P. Nason, and C. Oleari, "Matching NLO QCD computations with parton shower simulations: the POWHEG method", *JHEP* **11** (2007) 070, doi:10.1088/1126-6708/2007/11/070, arXiv:0709.2092.

[32] S. Alioli, P. Nason, C. Oleari, and E. Re, "A general framework for implementing NLO calculations in shower Monte Carlo programs: the POWHEG BOX", *JHEP* **06** (2010) 043, doi:10.1007/JHEP06(2010)043, arXiv:1002.2581.

[33] S. Alioli et al., "Jet pair production in POWHEG", *JHEP* **04** (2011) 081, doi:10.1007/JHEP04(2011)081, arXiv:1012.3380.

[34] S. Alioli, P. Nason, C. Oleari, and E. Re, "NLO Higgs boson production via gluon fusion matched with shower in POWHEG", *JHEP* **04** (2009) 002, doi:10.1088/1126-6708/2009/04/002, arXiv:0812.0578.

[35] G. Luisoni, P. Nason, C. Oleari, and F. Tramontano, "$HW^{\pm}/HZ + 0$ and 1 jet at NLO with the POWHEG BOX interfaced to GoSam and their merging within MiNLO", *JHEP* **10** (2013) 083, doi:10.1007/JHEP10(2013)083, arXiv:1306.2542.

[36] D. de Florian, G. Ferrera, M. Grazzini, and D. Tommasini, "Higgs boson production at the LHC: transverse momentum resummation effects in the $H \to \gamma\gamma$, $H \to WW \to l\nu l\nu$ and $H \to ZZ \to 4l$ decay modes", *JHEP* **06** (2012) 132, doi:10.1007/JHEP06(2012)132, arXiv:1203.6321.

[37] M. Grazzini and H. Sargsyan, "Heavy-quark mass effects in Higgs boson production at the LHC", *JHEP* **09** (2013) 129, doi:10.1007/JHEP09(2013)129, arXiv:1306.4581.

[38] LHC Higgs Cross Section Working Group, "Handbook of LHC Higgs cross sections: 4. Deciphering the nature of the Higgs sector", doi:10.23731/CYRM-2017-002, arXiv:1610.07922.

[39] A. Denner et al., "Standard model Higgs-boson branching ratios with uncertainties", *Eur. Phys. J. C* **71** (2011) 1753, doi:10.1140/epjc/s10052-011-1753-8, arXiv:1107.5909.

[40] NNPDF Collaboration, "Impact of heavy quark masses on parton distributions and LHC phenomenology", *Nucl. Phys. B* **849** (2011) 296, doi:10.1016/j.nuclphysb.2011.03.021, arXiv:1101.1300.

[41] J. M. Campbell and R. K. Ellis, "MCFM for the Tevatron and the LHC", *Nucl. Phys. Proc. Suppl.* **205-206** (2010) 10, doi:10.1016/j.nuclphysbps.2010.08.011, arXiv:1007.3492.

[42] R. Frederix and S. Frixione, "Merging meets matching in MC@NLO", *JHEP* **12** (2012) 061, doi:10.1007/JHEP12(2012)061, arXiv:1209.6215.

[43] J. Alwall et al., "Comparative study of various algorithms for the merging of parton showers and matrix elements in hadronic collisions", *Eur. Phys. J. C* **53** (2008) 473, doi:10.1140/epjc/s10052-007-0490-5, arXiv:0706.2569.

[44] T. Sjöstrand et al., "An introduction to PYTHIA 8.2", *Comput. Phys. Commun.* **191** (2015) 159, doi:10.1016/j.cpc.2015.01.024, arXiv:1410.3012.

[45] R. D. Ball et al., "Unbiased global determination of parton distributions and their uncertainties at NNLO and at LO", *Nucl. Phys. B* **855** (2012) 153, doi:10.1016/j.nuclphysb.2011.09.024, arXiv:1107.2652.

[46] CMS Collaboration, "Event generator tunes obtained from underlying event and multiparton scattering measurements", *Eur. Phys. J. C* **76** (2016) 155, doi:10.1140/epjc/s10052-016-3988-x, arXiv:1512.00815.

[47] GEANT4 Collaboration, "GEANT4—a simulation toolkit", *Nucl. Instrum. Meth. A* **506** (2003) 250, doi:10.1016/S0168-9002(03)01368-8.

[48] CMS Collaboration, "Particle-flow reconstruction and global event description with the CMS detector", *JINST* **12** (2017) P10003, doi:10.1088/1748-0221/12/10/P10003, arXiv:1706.04965.

[49] M. Cacciari, G. P. Salam, and G. Soyez, "FastJet user manual", *Eur. Phys. J. C* **72** (2012) 1896, doi:10.1140/epjc/s10052-012-1896-2, arXiv:1111.6097.

[50] M. Cacciari and G. P. Salam, "Dispelling the N^3 myth for the k_T jet-finder", *Phys. Lett. B* **641** (2006) 57, doi:10.1016/j.physletb.2006.08.037, arXiv:hep-ph/0512210.

[51] CMS Collaboration, "Performance of missing transverse momentum in pp collisions at $\sqrt{s}$=13 TeV using the CMS detector", CMS Physics Analysis Summary CMS-PAS-JME-17-001, 2018.

[52] M. Cacciari, G. P. Salam, and G. Soyez, "The anti-k_T jet clustering algorithm", *JHEP* **04** (2008) 063, doi:10.1088/1126-6708/2008/04/063, arXiv:0802.1189.

[53] H. Voss, A. Höcker, J. Stelzer, and F. Tegenfeldt, "TMVA, the toolkit for multivariate data analysis with ROOT", in *XI Int. Workshop on Advanced Computing and Analysis Techniques in Physics Research*. 2007. arXiv:physics/0703039.

[54] CMS Collaboration, "Performance of electron reconstruction and selection with the CMS detector in proton-proton collisions at $\sqrt{s} = 8$ TeV", *JINST* **10** (2015) P06005, doi:10.1088/1748-0221/10/06/P06005, arXiv:1502.02701.

[55] CMS Collaboration, "Performance of the CMS muon detector and muon reconstruction with proton-proton collisions at $\sqrt{s} = 13$ TeV", *JINST* **13** (2018) P06015, doi:10.1088/1748-0221/13/06/P06015, arXiv:1804.04528.

[56] CMS Collaboration, "Identification of heavy-flavour jets with the CMS detector in pp collisions at 13 TeV", *JINST* **13** (2017) P05011, doi:10.1088/1748-0221/13/05/P05011, arXiv:1712.07158.

[57] CMS Collaboration, "Reconstruction and identification of τ lepton decays to hadrons and ν_τ at CMS", *JINST* **11** (2016) P01019, doi:10.1088/1748-0221/11/01/P01019, arXiv:1510.07488.

[58] CMS Collaboration, "Performance of reconstruction and identification of tau leptons in their decays to hadrons and tau neutrino in LHC Run-2", CMS Physics Analysis Summary CMS-PAS-TAU-16-002, 2016.

[59] CMS Collaboration, "Performance of reconstruction and identification of τ leptons decaying to hadrons and ν_τ in pp collisions at $\sqrt{s} = 13$ TeV", *JINST* **13** (2018), no. 10, P10005, doi:10.1088/1748-0221/13/10/P10005, arXiv:1809.02816.

[60] CMS Collaboration, "Measurement of the inclusive W and Z production cross sections in pp collisions at $\sqrt{s} = 7$ TeV", *JHEP* **10** (2011) 132, doi:10.1007/JHEP10(2011)132, arXiv:1107.4789.

[61] J. Butterworth et al., "PDF4LHC recommendations for LHC Run II", *J. Phys. G* **43** (2016) 023001, doi:10.1088/0954-3899/43/2/023001, arXiv:1510.03865.

[62] CMS Collaboration, "Measurement of the cross section for top quark pair production in association with a W or Z boson in proton-proton collisions at $\sqrt{s} = 13$ TeV", (2017). arXiv:1711.02547. Submitted to *JHEP*.

[63] CMS Collaboration, "Performance of missing energy reconstruction in 13 TeV pp collision data using the CMS detector", CMS Physics Analysis Summary CMS-PAS-JME-16-004, 2016.

[64] CMS Collaboration, "CMS luminosity measurements for the 2016 data taking period", CMS Physics Analysis Summary CMS-PAS-LUM-17-001, 2017.

[65] A. L. Read, "Presentation of search results: The CL_s technique", *J. Phys. G* **28** (2002) 2693, doi:10.1088/0954-3899/28/10/313.

[66] T. Junk, "Confidence level computation for combining searches with small statistics", *Nucl. Instrum. Meth. A* **434** (1999) 435, doi:10.1016/S0168-9002(99)00498-2, arXiv:hep-ex/9902006.

[67] ATLAS and CMS Collaborations, The LHC Higgs Combination Group, "Procedure for the LHC Higgs boson search combination in Summer 2011", Technical Report CMS-NOTE-2011-005. ATL-PHYS-PUB-2011-11, 2011.

[68] G. Cowan, K. Cranmer, E. Gross, and O. Vitells, "Asymptotic formulae for likelihood-based tests of new physics", *Eur. Phys. J. C* **71** (2011) 1554, doi:10.1140/epjc/s10052-011-1554-0, arXiv:1007.1727. [Erratum: doi:10.1140/epjc/s10052-013-2501-z].

[69] S. Heinemeyer, W. Hollik, and G. Weiglein, "FeynHiggs: A program for the calculation of the masses of the neutral CP-even Higgs bosons in the MSSM", *Comput. Phys. Commun.* **124** (2000) 76, doi:10.1016/S0010-4655(99)00364-1, arXiv:hep-ph/9812320.

[70] S. Heinemeyer, W. Hollik, and G. Weiglein, "The masses of the neutral CP-even Higgs bosons in the MSSM: Accurate analysis at the two-loop level", *Eur. Phys. J. C* **9** (1999) 343, doi:10.1007/s100529900006, arXiv:hep-ph/9812472.

[71] G. Degrassi et al., "Towards high-precision predictions for the MSSM Higgs sector", *Eur. Phys. J. C* **28** (2003) 133, doi:10.1140/epjc/s2003-01152-2, arXiv:hep-ph/0212020.

[72] M. Frank et al., "The Higgs boson masses and mixings of the complex MSSM in the Feynman-diagrammatic approach", *JHEP* **02** (2007) 047, doi:10.1088/1126-6708/2007/02/047, arXiv:hep-ph/0611326.

[73] T. Hahn et al., "High-precision predictions for the light CP-even Higgs boson mass of the minimal supersymmetric standard model", *Phys. Rev. Lett.* **112** (2014) 141801, doi:10.1103/PhysRevLett.112.141801, arXiv:1312.4937.

[74] R. V. Harlander, S. Liebler, and H. Mantler, "SusHi: A program for the calculation of Higgs production in gluon fusion and bottom-quark annihilation in the standard model and the MSSM", *Comput. Phys. Commun.* **184** (2013) 1605, doi:10.1016/j.cpc.2013.02.006, arXiv:1212.3249.

[75] M. Spira, A. Djouadi, D. Graudenz, and P. M. Zerwas, "Higgs boson production at the LHC", *Nucl. Phys. B* **453** (1995) 17, doi:10.1016/0550-3213(95)00379-7, arXiv:hep-ph/9504378.

[76] R. V. Harlander and M. Steinhauser, "Supersymmetric Higgs production in gluon fusion at next-to-leading order", *JHEP* **09** (2004) 066, doi:10.1088/1126-6708/2004/09/066, arXiv:hep-ph/0409010.

[77] R. Harlander and P. Kant, "Higgs production and decay: Analytic results at next-to-leading order QCD", *JHEP* **12** (2005) 015, doi:10.1088/1126-6708/2005/12/015, arXiv:hep-ph/0509189.

[78] G. Degrassi and P. Slavich, "NLO QCD bottom corrections to Higgs boson production in the MSSM", *JHEP* **11** (2010) 044, doi:10.1007/JHEP11(2010)044, arXiv:1007.3465.

[79] G. Degrassi, S. Di Vita, and P. Slavich, "NLO QCD corrections to pseudoscalar Higgs production in the MSSM", *JHEP* **08** (2011) 128, doi:10.1007/JHEP08(2011)128, arXiv:1107.0914.

[80] G. Degrassi, S. Di Vita, and P. Slavich, "On the NLO QCD corrections to the production of the heaviest neutral Higgs scalar in the MSSM", *Eur. Phys. J. C* **72** (2012) 2032, doi:10.1140/epjc/s10052-012-2032-z, arXiv:1204.1016.

[81] R. V. Harlander and W. B. Kilgore, "Next-to-next-to-leading order Higgs production at hadron colliders", *Phys. Rev. Lett.* **88** (2002) 201801, doi:10.1103/PhysRevLett.88.201801, arXiv:hep-ph/0201206.

[82] C. Anastasiou and K. Melnikov, "Higgs boson production at hadron colliders in NNLO QCD", *Nucl. Phys. B* **646** (2002) 220, doi:10.1016/S0550-3213(02)00837-4, arXiv:hep-ph/0207004.

[83] V. Ravindran, J. Smith, and W. L. van Neerven, "NNLO corrections to the total cross-section for Higgs boson production in hadron-hadron collisions", *Nucl. Phys. B* **665** (2003) 325, doi:10.1016/S0550-3213(03)00457-7, arXiv:hep-ph/0302135.

[84] R. V. Harlander and W. B. Kilgore, "Production of a pseudo-scalar Higgs boson at hadron colliders at next-to-next-to leading order", *JHEP* **10** (2002) 017, doi:10.1088/1126-6708/2002/10/017, arXiv:hep-ph/0208096.

[85] C. Anastasiou and K. Melnikov, "Pseudoscalar Higgs boson production at hadron colliders in next-to-next-to-leading order QCD", *Phys. Rev. D* **67** (2003) 037501, doi:10.1103/PhysRevD.67.037501, arXiv:hep-ph/0208115.

[86] U. Aglietti, R. Bonciani, G. Degrassi, and A. Vicini, "Two-loop light fermion contribution to Higgs production and decays", *Phys. Lett. B* **595** (2004) 432, doi:10.1016/j.physletb.2004.06.063, arXiv:hep-ph/0404071.

[87] R. Bonciani, G. Degrassi, and A. Vicini, "On the generalized harmonic polylogarithms of one complex variable", *Comput. Phys. Commun.* **182** (2011) 1253, doi:10.1016/j.cpc.2011.02.011, arXiv:1007.1891.

[88] R. V. Harlander and W. B. Kilgore, "Higgs boson production in bottom quark fusion at next-to-next-to leading order", *Phys. Rev. D* **68** (2003) 013001, doi:10.1103/PhysRevD.68.013001, arXiv:hep-ph/0304035.

[89] S. Dittmaier, M. Krämer, and M. Spira, "Higgs radiation off bottom quarks at the Fermilab Tevatron and the CERN LHC", *Phys. Rev. D* **70** (2004) 074010, doi:10.1103/PhysRevD.70.074010, arXiv:hep-ph/0309204.

[90] S. Dawson, C. B. Jackson, L. Reina, and D. Wackeroth, "Exclusive Higgs boson production with bottom quarks at hadron colliders", *Phys. Rev. D* **69** (2004) 074027, doi:10.1103/PhysRevD.69.074027, arXiv:hep-ph/0311067.

[91] A. Djouadi, J. Kalinowski, and M. Spira, "HDECAY: A program for Higgs boson decays in the standard model and its supersymmetric extension", *Comput. Phys. Commun.* **108** (1998) 56, doi:10.1016/S0010-4655(97)00123-9, arXiv:hep-ph/9704448.

[92] A. Djouadi, M. M. Muhlleitner, and M. Spira, "Decays of supersymmetric particles: The program SUSY-HIT (SUspect-SdecaY-Hdecay-InTerface)", *Acta Phys. Polon. B* **38** (2007) 635, arXiv:hep-ph/0609292.

[93] A. Bredenstein, A. Denner, S. Dittmaier, and M. M. Weber, "Precise predictions for the Higgs-boson decay H$\to$ WW/ZZ $\to$ 4 leptons", *Phys. Rev. D* **74** (2006) 013004, doi:10.1103/PhysRevD.74.013004, arXiv:hep-ph/0604011.

[94] A. Bredenstein, A. Denner, S. Dittmaier, and M. M. Weber, "Precision calculations for the Higgs decays H $\to$ ZZ/WW $\to$ 4 leptons", *Nucl. Phys. Proc. Suppl.* **160** (2006) 131–135, doi:10.1016/j.nuclphysbps.2006.09.104, arXiv:hep-ph/0607060.

[95] A. Bredenstein, A. Denner, S. Dittmaier, and M. M. Weber, "Radiative corrections to the semileptonic and hadronic Higgs-boson decays H $\to$ WW/ZZ $\to$ 4 fermions", *JHEP* **02** (2007) 080, doi:10.1088/1126-6708/2007/02/080, arXiv:hep-ph/0611234.